Regular Article

PHYSICAL CHEMISTRY RESEARCH
Published by the
Iranian Chemical Society
www.physchemres.org
info@physchemres.org

Phys. Chem. Res., Vol. 8, No. 4, 629-644, December 2020
DOI: 10.22036/pcr.2020.224867.1748

A Reactive Molecular Dynamics Simulation of the Flame Synthesis of Silica Nanoparticles

M.E. Izadi and H. Sabzyan*

Department of Chemistry, University of Isfahan, Isfahan 81746-73441, I. R. Iran

(Received 29 March 2020, Accepted 28 June 2020)

Reactive molecular dynamics simulations (RMDS) with the ReaxFF force field are used to study nucleation and growth of silica nanoparticles during flame synthesis from tetramethoxysilane (TMOS). Two reactive systems (A and B) are considered and formation and/or consumption of various reactants, intermediates and products are followed. In the RMDSs of system A (TMOS, O_2, SiO_2 and Ar), the temperature-dependence of the formation of initial Si_mO_n seeds show that formation of transient $SiO_3C_3H_9$ intermediate is an important stage in the conversion of TMOS to the initial Si_mO_n seeds, which then aggregate to produce silica nanoparticles. Increasing temperature speeds up this conversion. Results of the RMDSs on system B (TMOS, O_2, Ar and $\{Si_mO_n\}$; the Si_mO_n seeds play the role of the initial silica nanoparticles) show that at 2100 K, application of weak EFs (~1 V/Å) narrows the size distribution of the silica nanoparticles compared to that in the absence of EF while by application of stronger EFs (4-8 V/Å), the initial Si_mO_n nanoparticles split into smaller species. In the absence of EF, increasing temperature from 1500 K to 3000 K increases sizes of the nanoparticles. The radial distribution functions, coordination numbers, and atomic compositions are used to characterize nanoparticles and evolution of the reaction.

Keywords: Reactive molecular dynamics simulation, Silica nanoparticle, Flame synthesis, Nucleation, Electric field

INTTRODUCTION

Nanostructures, including nanoparticles (NP), nanorods, nanowires, thin layers and nanostructure bulk materials have at least one nano-size dimension. Properties of nanostructures are related to their sizes, particle size distribution, shape, etc. So far, several methods have been developed for the efficient synthesis of nanostructures. The nanostructures can be prepared in different phases; *e.g.*, in vapor, liquid, solid or hybrid phases [1,2]. For the synthesis of a specific nanostructure, there may be a variety of chemical routes starting from different reactants under different chemical and physical conditions and post-treatments [3,4,5]. For improving production efficiency and quality of the products, the preparation methods should be optimized experimentally. With the emergence of computational and simulation methods, it is, however, possible to evaluate relative efficiency of different proposed experimental methods and screen out non-effective methods or even to predict the optimized conditions for a selected method within the computational and the model accuracies [6,7].

Fumed silica, with branch-like chain nanostructure and micrometer particle size, can be synthesized in flame. In the flame synthesis process (known also as flame spray pyrolysis, flame aerosol process) the synthesized primary particles collide and attach or connect to produce larger branchy particles [8-11].

Most of the reactions leading to nanostructure materials occur at interfaces and follow long-range spatiotemporal mechanisms. For example, producing self-assembled monolayers [12], thin films [13] and core-shell nanoparticles [14] are some common nanostructures resulting from interface chemical reactions through long-range spatiotemporal mechanisms. Understanding the mechanisms is critical for clever design of nanostructures with desired

*Corresponding author. E-mail: sabzyan@sci.ui.ac.ir

characteristics. Obviously, non-reactive classical molecular dynamics (MD) techniques are not able to simulate the behavior of reactive systems. For the detailed investigation of large-scale diffusive/convective reactive systems, especially at interfaces, the quantum mechanics-molecular dynamics (QMMD) methods are not applicable due to being costly time-wise and demanding advanced high-performance computational facilities [15]. The reactive force field ReaxFF introduced by van Duin *et al.* [16] has been developed such that, while having all advantages of an ordinary MD technique, it can also simulate reactive systems. Moreover, this force field is especially of interest in the simulation of nano-size reactive systems in order to reproduce results within acceptable accuracies expected from quantum computational methods. This reactive force field can thus be used for the study and simulation of the chemical reactions, particularly those engaged in the production of nanostructures. For example, this force field has so far been used to investigate carbon nanotubes (CNTs) production. In fact, there are several types of CNTs (*e.g.,* multi/single-wall CNTs with different chiralities, sizes and shapes) and for each type, different characteristics are simulated which are comparable with experimental reports [17,18].

So far, a number of computational techniques have been used to study silica, including modeling the flame synthesis of silica NPs [19,20], MD simulations of the competitive adsorption of siloxanes and water on the silica surface [21], ab initio study of hydroxylated silica clusters [22], MD simulation of the aggregation of nanocolloidal amorphous silica [23] and QMMD study of poly(dimethylsiloxane)-silica NP interactions [24]. Van Duin *et al.* [25] developed a reactive force field for silicon and silicon oxide systems. Since then, the ReaxFF software has been used for the study of the silica-water interface [26], investigation of oxygen interaction with silicon surface [20,27], study of the silicon/silicon oxide interface in silicon nanowires and bulk structure [28,29], thermal decomposition of a poly(dimethylsiloxane) polymer [30], investigation of physicochemical process of collision of the high velocity ice clusters on silica surfaces [31], reactive molecular dynamics (RMD) simulation of the silica-water interactions in nanoscale pores in comparison with quantum mechanical molecular dynamics (QM-MD) simulation [32,33], and RMD investigation of the hydroxylation process on strained silica nano wires and amorphous silica slab [34].

Effect of the external electric field (EF) was investigated in the synthesis of some nanomaterials, *e.g.,* in the flame synthesis of titania NPs [11,35-37], and flame synthesis [38] and chemical vapor deposition [39] of carbon nanotubes. In the flame process, the applied electric field can control aggregation and sizes of primary particles; EF usually decreases the particle size of the products [40-42]. In addition, a number of RMD simulation works were reported in the literature [43,44] in which the effect of electric field on reactive chemical systems have been investigated. By applying external EF, using a simple experimental setup, characteristics of the particles can be controlled. Ions and electrons produced during a flame synthesis under an EF, attach to reactants, intermediates, and products and produced new charged species which can further be affected by the applied EF, and flown towards the electrodes. Therefore, the collision schemes is changed due to, for example, spreading away from the concentrated region of the flow, and leading to less collisions and aggregation of the particles. As a consequence, the EF also increases the temperature and alters structure (width and height) of the flame. In this way, application of EF changes the time duration over which particles experience the high-temperature region of the flame [34,45,46].

Considering extensive and growing applications of fumed silica, optimization of the chemical and physical conditions for efficient synthesis of silica nanoparticles (NPs) with properties of interest for specific new applications such as fillers, synthesis of magnetorheological fluids and emulsions is of great importance [47-49]. In this paper, the results of the reactive molecular dynamic simulations carried out on the fumed silica synthesis are reported. These simulations aim to obtain information on silica NPs growth in the flame, the application of the EF, and the temperature influence on the process. For this purpose, the effects of EF and temperature on the attachment of fumed silica NPs in the flame synthesis process in the presence of tetramethoxysilane (TMOS) as a precursor, have been investigated by RMD simulations based on a reactive force field containing parameters optimized for the {Si/O/H} systems [50].

COMPUTATIONS

ReaxFF Force Field

In the ReaxFF force field, there are two sets of potential functions, one for the valance interactions and the other for nonbonding interactions, which are added to calculate the total potential energy as:

$$E_{system} = E_{bond} + E_{under} + E_{over} + E_{lp} + E_{val} + E_{tor} + E_{vdWaals} + E_{Coulomb}$$

Partial energy contributions appearing in this summation comprise bond (E_{bond}), under-coordination (E_{under}), over-coordination (E_{over}), lone pair (E_{lp}), valance angle (E_{val}), torsion angle (E_{tor}), van der Waals ($E_{vdWaals}$) and coulomb ($E_{Coulomb}$) energies. The total potential energy may include more terms taking care of special bonding and non-bonding interactions. The ReaxFF force field distinguishes between contributions of sigma, pi- and double pi- bonds, in which bond energies vary with inter-atomic distances. In this force field, Coulomb and van der Waals interactions are considered between all pairs of atoms of the systems under study. The partial charges are dependent on the interatomic distances, and are calculated at each time step of the simulation using a charge-equilibration scheme [23]. In this study, we used the optimized ReaxFF force field with the parameters fitted to 304 reference structures including a mixture of species, ranging from simple silanes to quartz, and a group of 309 reference properties such as geometry data, partial charges, crystal cell parameters, and relative energies [39].

Simulation Box Details

Two reactive systems have been investigated in the present study. System A is intended for the RMD simulation of the silica NPs nucleation from silica precursors at different temperatures. For this purpose, 61 TMOS and 50 SiO_2 gas-phase molecules (precursors, as the source of Si and O atoms), 350 O_2 molecules (as oxidant) and 20 Ar atoms (as inert gas) are considered as the initial composition. System B is designed to carry out simulations of the growth or binding of silica NPs. Composition of this system includes 22 spherical stoichiometric silica (SiO_2) NPs, 21 TMOS precursor molecules, 179 O_2 oxidant molecules and 20 inert Ar atoms. The A and B systems thus contain totals of 2151 and 2073 atoms, respectively, and in both, all fragments (NPs and molecules) are randomly distributed over the whole space of the cubic simulation box. To maintain constant pressure, the box size (a) is adjusted at each temperature. Details of the simulation box are summarized in Table 1.

All of the simulations were carried out in an NVT ensemble with a time step of 0.1 fs and total number of steps of 10×10^6 and 6×10^6 for the A and B systems (equivalent to 1.0 and 0.6 ns), respectively. Also, the Nosé-Hoover thermostat with a temperature-damping constant of 10 fs is used to maintain an isothermal reaction condition. For geometry optimization of the initial state of both systems, the conjugate gradient energy minimization algorithm is used. For this purpose, for each simulation, convergence criteria of either force ($\delta f_{max} = 1 \times 10^{-6}$ kcal mol^{-1} Å) or energy ($\delta E/E_{tot} = 1 \times 10^{-4}$), whichever comes first, is considered. To suppress or limit any biased results, 4 independent simulations with different initial geometries and spatial distributions have been carried out for each set of conditions. The average results obtained for 4 simulations at each temperature and EF strength are also reported. All simulations of the present study are carried out with the LAMMPS software [51].

Electric Field Effect

Based on the typical chemical bond potential energy curves and energies, and the range of electric field (EF) strengths used in previous studies reported in literature [11,37-42,43-46], the EF range of 0-8 V/Å is found appropriate for our present reactive system. For the evaluation of the field-effect, in the preliminary stage of this study, the reactive system B is simulated (at 2100 K only) under EFs of different strengths 1, 2, 3, 4, 5, 6, 7 and 8 V/Å. It is found that in the EFs below 1 V/Å strength, no reaction occurs in the system. By increasing the EF strength, reactants undergo reactive collisions and the number of fragments in the system increases. In very strong Efs (7 V/Å and higher), the simulation system becomes unstable and all initial fragments decompose into atoms or very small clusters.

Table 1. Details of the Simulations of the A and B Systems Described in the Text

System	Reactants	Chemical formula	Number of reactants	Temperature (K)	Box size a (Å)	Density (mg cm^{-3})
A	SiO_2 (g)	SiO_2	50	1500	350	0.941
	TMOS	$Si(OCH_3)_4$	61	2100	390	0.680
	Oxygen	O_2	350	2700	430	0.507
	Argon	Ar	20	3300	470	0.389
B				1500	350	1.350
	Spherical SiO_2 NP	$Si_{19}O_{38}$	22	2100	390	0.980
	TMOS	$Si(OCH_3)_4$	21	2400	410	0.840
	Oxygen	O_2	179	2700	430	0.728
	Argon	Ar	20	3000	450	0.635
				3300	470	0.557

RESULTS AND DISCUSSION

System A

To analyze the evolution of system A during the simulations, chemical composition (numbers and types of species) is printed every 250 steps (*i.e.,* 25 fs) and is averaged over 4 independent simulations. These results are used to derive total number of species over the whole course of 1 ns RMD simulation at each temperature. For brevity, analysis of the data is carried out on the species present in more than 10000 (out of a total of 40000) sampled compositions. The number of species meeting this criterion are followed with time and plotted in Fig. 1. As shown in this Figure, the TMOS, O_2 and SiO_2 species, introduced as precursors, are consumed as the reaction proceed. Increasing temperature increases consumption rate of these species. The TMOS precursor is decomposed in the early stage of simulation into $SiO_3C_3H_9$, $SiO_3C_3H_8$, $SiO_3C_2H_6$, CH_3O, CH_2O, CH_3 and H species (see parts d-j of Fig. 1). In the later stages of simulation, these species are decomposed gradually by losing their carbon and hydrogen atoms (See Fig. S1 of the Supporting Information), and produce the initial SiO_2 seeds of less than 14 atoms. The detailed mechanism of the TMOS degradation can be worked out upon detailed analysis of all constituting reactions occurring in this reactive system if the simulations are carried out for a statistically large number of different compositions, distributions, densities and simulation box sizes. This massive work is beyond the scope of the present work. Therefore, only at 2700 K, decomposition of TMOS to $SiO_3C_3H_9$, $SiO_3C_3H_8$, $SiO_3C_2H_6$, CH_3O, CH_3 and H species have been followed over the first half part (0.5 ns) of the 1 ns simulation, occurring *via* the following three net reactions.

1. $Si(OCH_3)_4 \rightarrow SiO_3C_3H_9 + OCH_3$
2. $SiO_3C_3H_9 \rightarrow SiO_3C_2H_6 + CH_3$
3. $SiO_3C_3H_9 \rightarrow SiO_3C_3H_8 + H$

In fact, they include reverse reactions as well. So, they contain information about production and consumption of all species participating in these reactions. It is found that within the first 0.5 ns, 30 of the TMOS molecules are

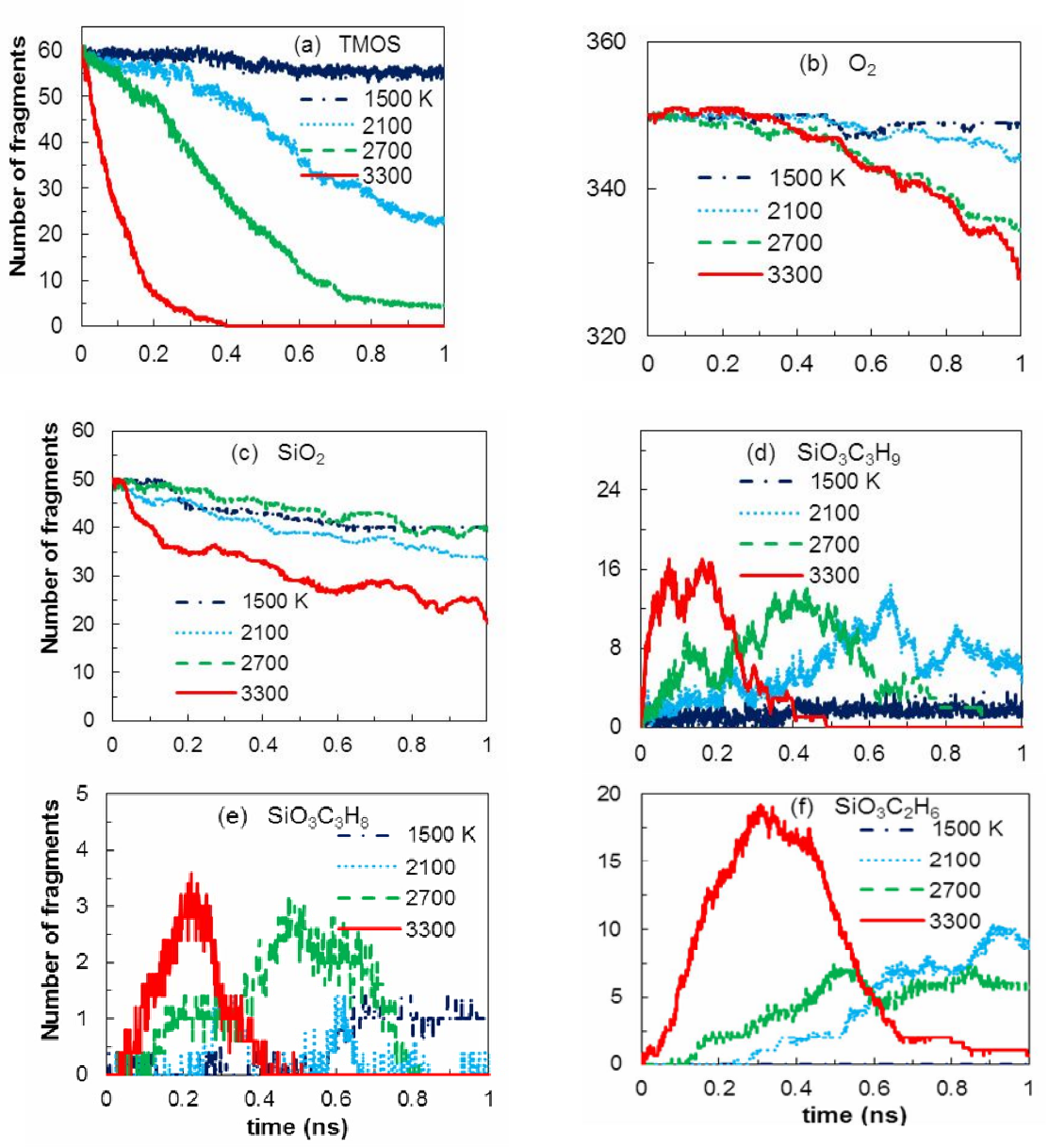

Fig. 1. Variations of the number of TMOS, SiO_2 and O_2 molecules (a, b, c) and $SiO_3C_3H_9$ (d), $SiO_3C_3H_8$ (e), $SiO_3C_2H_6$ (f), CH_3O (g), CH_2O (h), CH_3 (i) and H (j) fragments resulted from the decomposition of the TMOS molecules during 1 ns NVT RMD simulation of the system A (Table 1) at different temperatures. These results are averaged over 4 independent simulations with different initial geometries (distributions).

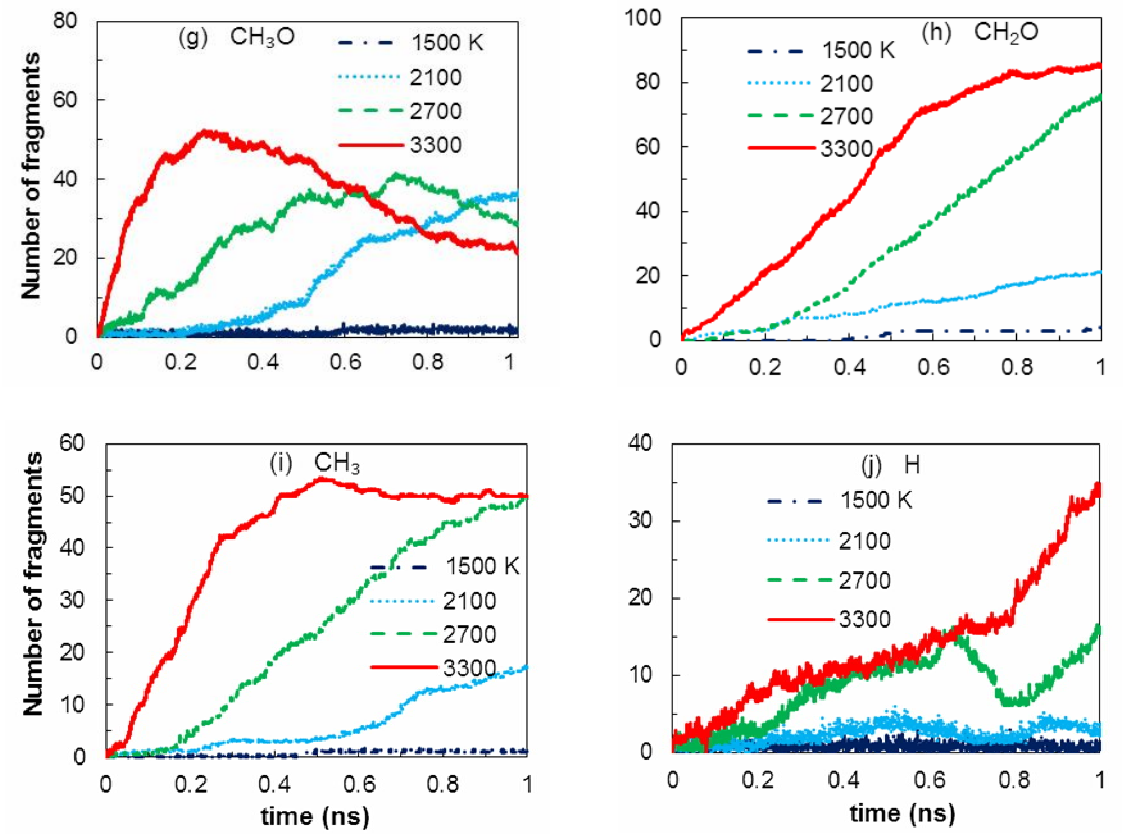

Fig. 1. Continued.

Table 2. Average Characteristics of the Silica Nuclei (Clusters) Produced after 1 ns RMD Simulations Performed for System A

T (K)	(m + n) in each Si_mO_n Nucleus	Number of Si_mO_n Nuclei	Sum of (m + n) in all Si_mO_n Nuclei
1500	6	4.25	56
	7	2	
	8	1.25	
	9	0.25	
	17	0.25	
2100	6	4.75	37.75
	7	0.75	
	8	0.5	
2700	6	1.75	10.5
3300	6	1	8
	8	0.25	

Nuclei (clusters) containing at least six Si and O atoms are considered only

converted to $SiO_3C_3H_9$ (in the 1st reaction) and then 16 of the $SiO_3C_3H_9$ fragments are decomposed to $SiO_3C_2H_6$ (*via* the 2nd reaction), while the 3rd reaction is not observed for this case.

The consumption rate of the O_2 molecule increases with time denoting appearance of more species having reaction tendency with this oxidant. The time-dependent concentration of the SiO_2 species (Fig. 1c), having no well-defined kinetics, shows that this species is consumed via several reaction pathways. Furthermore, the transient concentration (pile-up) of the $SiO_3C_3H_9$ species has two peaks (Fig. 1d) denoting its transient production *via* two reaction paths with different kinetics. The time lag between these two peaks decreases with increasing temperature. It seems that decomposition of this species results in the two $SiO_3C_3H_8$ and $SiO_3C_2H_6$ species (Figs. 1e and f). A similar behavior is observed for these species but with delays and smaller concentrations. As can be seen in Fig. 1g, pile-up of the OCH_3 species becomes higher and is shifted to shorter times as temperature increases. These changes show that while all reaction rates are increased with temperature, the rates of the reactions consuming this species increase faster than the rates of the reactions producing it.

It should be noted that several isomers may exist for each stoichiometry of the species in Fig. 1, and thus all of them are considered in the enumerations. Therefore, complex time-dependent behavior of the number of these species can be attributed, at least partly, to the superposition of the time-dependent number of their isomers. Therefore, in this study, we have tried to represent some examples of the capability of reactive simulations using ReaxFF in investigating chemical reactions. A complete and detailed investigation of the mechanism of this complex flame reaction (including all reactions and all possible species and their isomers), which is beyond the scope of the present work, remains to be accomplished in the continuation of the present study.

The SiO_2 clusters/nuclei produced during the 1n simulations are presented in Table 2 for each temperature. Note that only the clusters containing at least six Si and O atoms are considered as SiO_2 initial seed (nucleus). As can be seen from Table 2, the chemical type (stoichiometries) of the SiO_2 nuclei species has the highest diversity at the lowest temperature of 1500 K and by increasing the temperature this diversity is reduced. Moreover, the size (m + n) of the nuclei is decreased by increasing temperature. At 3300 K, the number of silica nuclei formed in the simulation is lowest which shows unfavored conditions for the SiO_2 nucleation from TMOS and SiO_2 molecules as precursors. At high temperatures (*e.g.* 3300 K), the species have high kinetic energies and velocities which either do not allow enough long interaction periods and need requirements for the establishment of chemical bonds, or result in sampling the interaction repulsion wall. In a real system under similar conditions and at this high temperature, Ar atoms can normally produce a plasma, while, in the present study, the Ar atoms are considered inert and un-ionizable since the ReaxFF force field does not include electrons. Therefore, the Ar atoms act only as a thermalizing agent regulating temperature of the gaseous reaction mixture during the present simulations. Furthermore, for consistency, all simulations should be carried out at similar conditions, and therefore, Ar atoms should be present in all simulations carried out at different temperatures.

System B

Details of the average number of fragments and NPs obtained from the simulations carried out on the system B at different conditions are reported in Table 3. The initial total number of NPs in this system was 22.

To follow the aggregation (growth) and/or fragmentation of NPs as functions of temperature and EF, Si and O contents within the NPs, Si(O) coordination number and size distribution of NPs are investigated for this system. At the end of the simulations (at 0.6 ns), the average contents of Si and O in NPs and coordination number of the Si(O) atoms (extracted from the radial distribution functions derived from simulations) versus temperature and EF strengths are depicted in Figs. 2 and 3, respectively. The Si(O) coordination number is calculated by integrating the first peak of the Si-O RDF (See Fig. 4, as an example). Moreover, histogram of the NP sizes (in terms of the average number of Si and O atoms) against temperature and EF intensity are demonstrated in Figs. 5 and 6, respectively. Here, also the same criteria are used for enumeration of the SiO_2 seeds (nuclei) as used for the analysis of the results of the system A.

Table 3. Average Number of Fragments and NPs Obtained after 0.6 ns NVT Simulations Carried out on System B (Table 1). For all Simulations, the Initial Total Number of NPs and Fragments were 22 and 242, Respectively

	T (K)	Total number of fragments	Total number of NPs[a]
(a) EF = 0	1500	278	20
	2100	460	19
	2400	304	20
	2700	406	19
	3000	438	21
	3300	489	28
	EF (V/Å)	Total number of fragments	Total number of NPs[a]
(b) T = 2100 K	1	256	22
	2	276	21
	3	326	21
	4	476	23
	5	596	23
	6	740	20
	7	904	12
	8	982	3

[a]The NPs have different sizes.

The average of radial distribution functions of the Si-Si, O-O and Si-O pairs of atoms in the system B at 1500 K and different temperatures and EFs is calculated and plotted in Fig. 4a and S2 (of the Supporting Information file), respectively. Moreover, to have a comparison with other studies reported on silica, the RDF curve in Fig. 2 of Ref. [52] is reproduced in Fig. 4b.

Temperature effect. As can be seen in Figs. 2a and 3a, increasing temperature (at EF = 0) from 1500 to 3300 K reduces the Si/O atom contents of NPs from 517/496 to 448/363, and reduces the Si(O) coordination number from 3.8 to 3.2. Analysis of the data reported in Table 3 and the histograms demonstrated in Fig. 5 shows that increasing temperature from 1500 K to 3000 K increases the size distribution of NPs due to the attachment of smaller NPs as a result of the faster random movements and more collisions. In addition, at 2400 and 3000 K, two new larger NPs are produced by attachment of smaller NPs present at 1500 K. Further increasing of temperature to 3300 K results in the dominant fragmentation of the NPs (see also

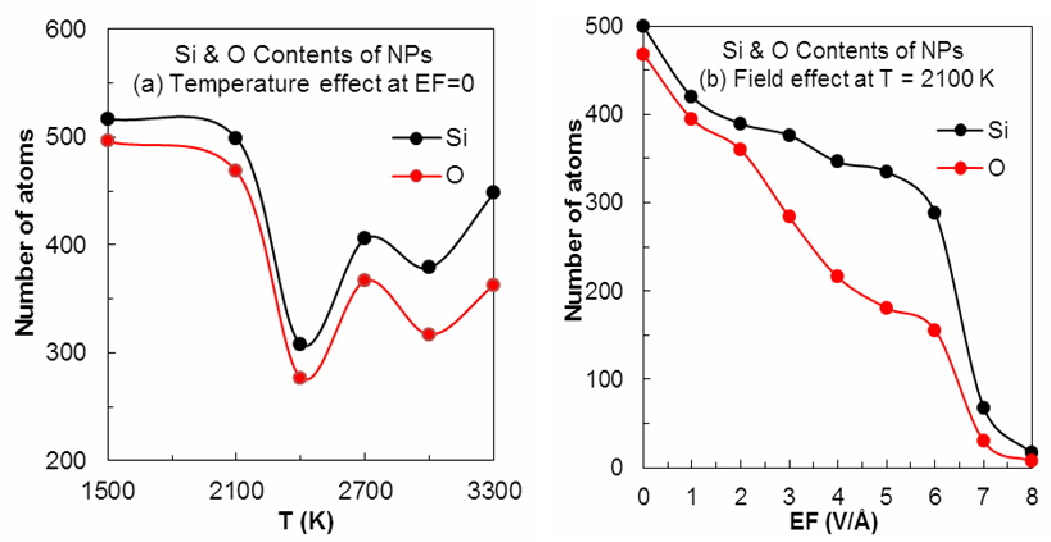

Fig. 2. The average contents of Si and O atoms in NPs after 0.6 ns NVT RMD simulation of system B (described in Table 1): (a) temperature effect in the absence of EF and (b) EF effect (applied along the *x*-direction) at the fixed temperature of 2100 K.

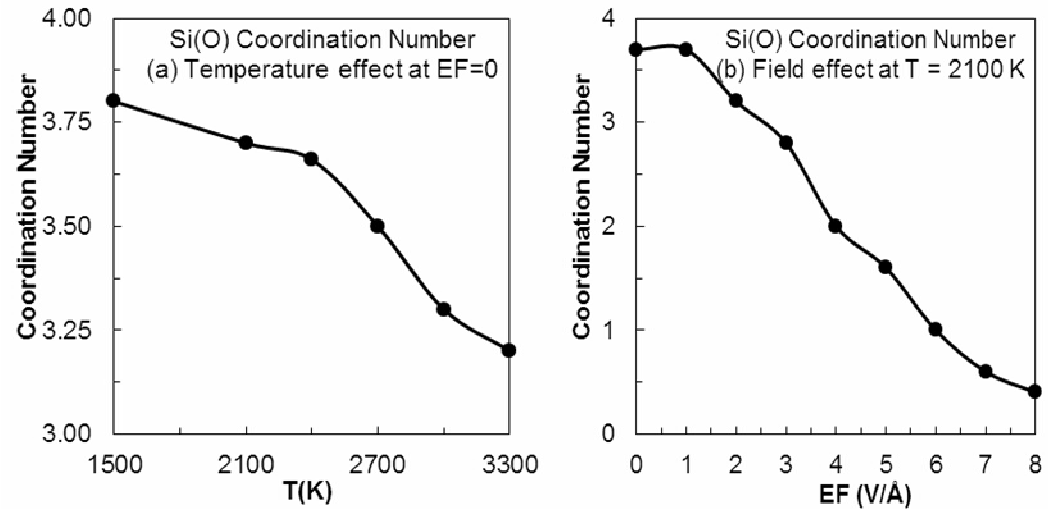

Fig. 3. Average coordination number of the oxygen atoms around the Si atom, Si(O), calculated by integration over the first peak of the Si-O RDF graphs obtained after 0.6 ns NVT RMD simulation of the system B: (a) temperature effect in the absence of EF and (b) EF effect applied along the *x*-direction at the fixed temperature of 2100 K.

Fig. S3a and S4a in the Supporting Information file). According to Fig. 5, at the lower temperature of 1500 K, NPs attach to produce larger NPs, and therefore, there remain two main sizes of NPs at the end of the simulations. At increased temperatures of 3000 and 3300 K, fragmentation and agglomeration act simultaneously over

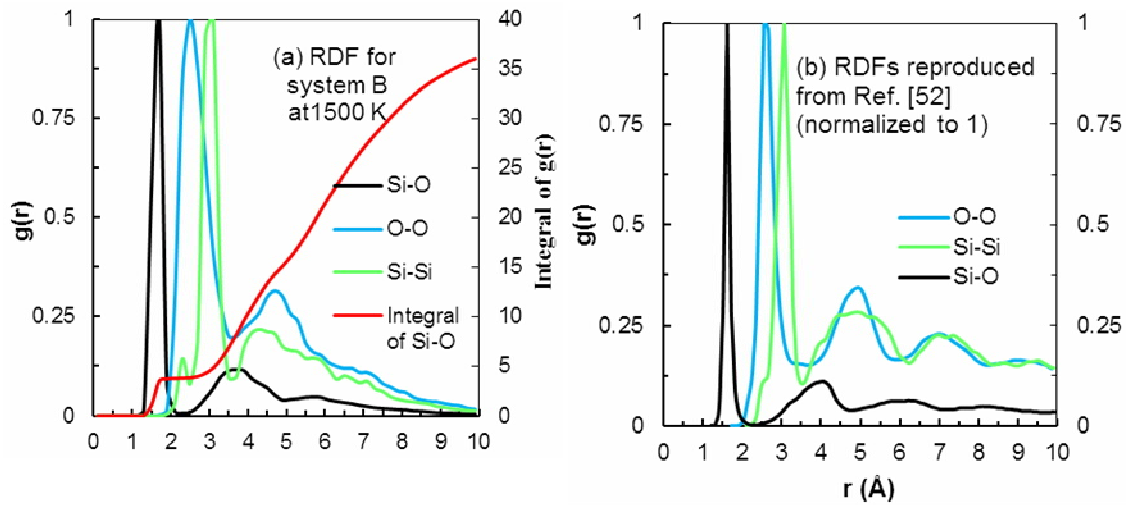

Fig. 4. The Si-O (black), O-O (blue) and Si-Si (green) radial distribution functions (RDF) calculated for the configuration of system B (Table 1) obtained at the end of the 0.6 ns NVT RMD simulation at 1500 K temperature, using an increment of $\Delta r = 0.2$ Å (a), and reproduced (with permission) from Ref. [52] (b). The integral of Si-O RDF curve (red) is also calculated and depicted in part (a) of the figure.

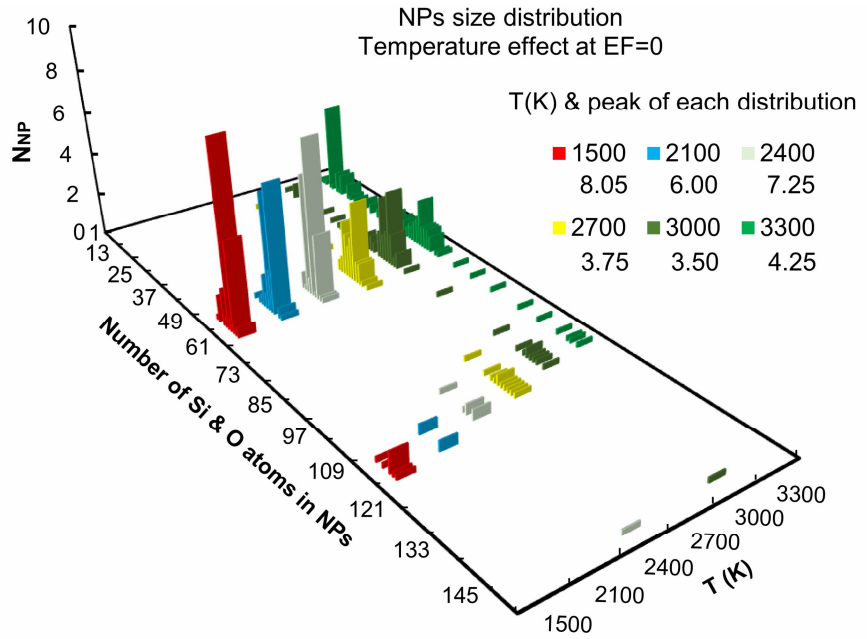

Fig. 5. The average NPs size histogram of the system B (Table 1) after 0.6 ns NVT RMD simulation at different temperatures in EF = 0. A minimum number of 6 interconnected Si and O atoms is considered as the lower limit to consider the cluster as NP.

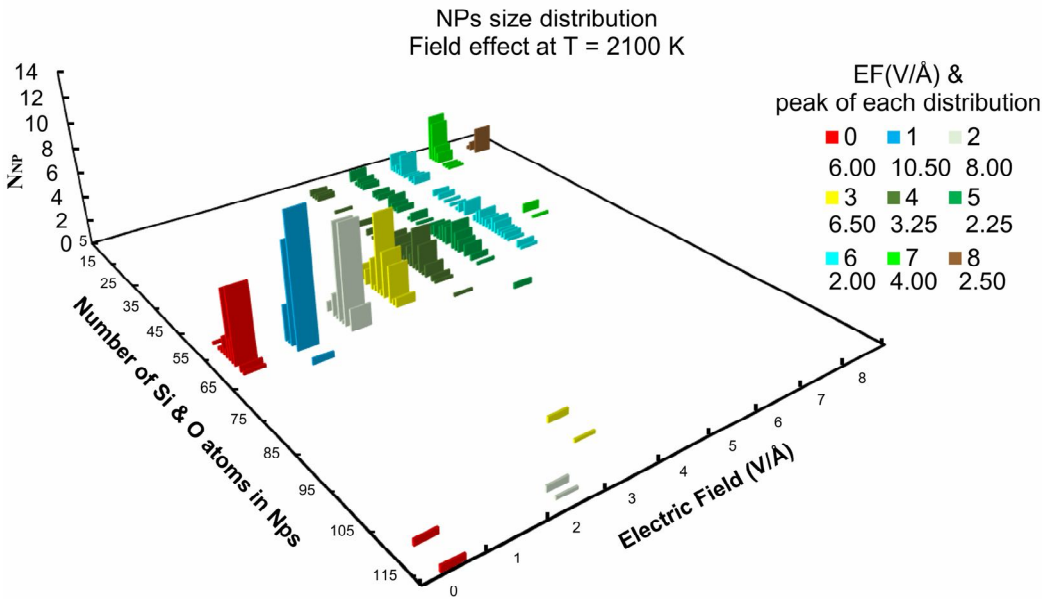

Fig. 6. Average NP size histogram of system B (Table 1) after 0.6 ns NVT RMD simulation at 2100 K at different EF strengths applied along the *x*-direction. A minimum number of 6 interconnected Si and O atoms is considered as criterion to consider the cluster as NP.

the simulations, and as a result, NPs of various sizes may be produced.

It can be deduced from Fig. 4 that the silica NPs formed in the system B has an amorphous phase with a Si-O bond length close to the value of 1.62 Å. The mean Si-Si and O-O distances within the SiO_2 NPs, extracted from the RDF graphs (Fig. 4), are 3.10 and 2.50 Å, which are in very good agreement with what extracted from Fig. 2 of Ref. [52]; *i.e.*, 3.07 and 2.61 Å, respectively. This validates the overall configuration of the Si and O atoms in the SiO_2 NPs obtained in the present study. The obtained RDF curves from Ref. [52] are on a single silica NP with 200 SiO_2 units in a simulation box at 300 K temperature while in this study there are several dissimilar NPs with different sizes and shapes at 1500 K temperature, and therefore, the RDF peaks become broader. Moreover, as can be seen from Fig. 4, the RDF curves obtained in this study goes to zero at long distances, while the curves from Ref. [52] approach their corresponding asymptotic non-zero values. This distinct difference comes from the fact that the NPs considered in the present study have finite (small) sizes and their separations in the gaseous systems setup in this work is very large. This is while, for calculation of the RDFs for the silica particle considered in Ref. 52, we used PBC to extend the unit cell structure in the 3D space (*i.e.,* it is a bulk with infinite size).

As a general trend, the RDF peaks are broadened at higher temperatures [53] due to higher thermal energies available to the atoms which allow them to sample more points away from the equilibrium points of the potential curves corresponding to the bond and bond angles. In the RDF of the Si-Si pair at 1500 K (shown in Fig. S2a), there are three peaks around 2.3, 2.9 and 4.5 Å, while at 3300 K, only two peaks appear around 2.9 and 4.3 Å. Increasing temperature results in NPs richer in Si which thus contain larger number of direct Si-Si bonds (corresponding to the first weak peak of the Si-Si RDF) with more diverse and increased lengths. Therefore, by increasing temperature, height of the first peak of the Si-Si RDF increases and merges into the most intense second peak (corresponding to the Si-O-Si bond sequence) which is also broadened at higher temperatures. Because of the attachment of NPs at higher temperatures, the height of the first peak of the O-O RDF, which corresponds to the O-Si-O bond sequence,

increases.

Electric field effect. As can be seen in Figs. 2b and 3b, increasing EF strength (at 2100 K) from 0 to 8 V/Å, reduces the Si/O atom contents from 499/468 to 16.3/7.4, and reduces the Si(O) coordination number sharply from 3.7 to 0.4. By reviewing the data reported in Table 3 and the histograms demonstrated in Fig. 6, it can be deduced that application of an external EF of 1 V/Å strength at 2100 K prevents attachment of the silica NPs, while at EFs of 1-2 V/Å strengths it seems that the NPs become more reactive and attach to produce larger NPs. At higher EFs in the range of 4-8 V/Å strengths, larger NPs are decomposed into smaller NPs and atomic and molecular species. A comparative analysis shows that the effect of EFs with ~7-8 V/Å strengths on the fragmentation of NPs at 2100 K is much stronger than that in the absence of EF at the 3300 K temperature (See Figs. S3, S4 and S5 in Supporting Information). This suggests that EF and temperature can be used alternatively to adjust characteristics of the particles produced in a flame synthesis. According to Fig. 6, narrowest size distribution of NPs is obtained in EF of 1 V/Å at 2100 K.

In the presence of EFs of around 1 V/Å strength, the charged particles move directionally and the dipolar species are oriented along the EF, and therefore, their random collisions and aggregations become less probable resulting in constant NPs. At EFs above 3 V/Å, the applied field becomes strong enough to induce breakage of the chemical bonds. For example, at 2100 K, in the 6 V/Å EF the number of O and Si atoms of the NPs drops from 499 and 468 atoms (in the absence of EF) to 288 and 155.8 atoms, respectively, while the number of nanoparticles (19 and 20) is almost the same.

Effects of the EF on the RDF curves at 2100 K are depicted in part (b) of Fig. S2 (Supporting Information). It can be seen from this Figure that the RDF curves undergo much deeper changes by increasing EF strength. For example, heights of the outer peaks of the Si-Si and O-O RDFs decrease effectively with increasing EF, which is mainly due to the decomposition of the NPs at higher EF. Specifically, at EF = 7 or 8 V/Å, all higher peaks disappear and only the first peak remains, showing that only small molecular (cluster) systems remain alive at these high EF strengths. These features and trends of the RDF curves observed in Fig. S2 are consistent with the size distribution of NPs observed in Fig. 6. Analysis of the EF effect on the Si-O RDF shows the same trends except that emergence of new diatomic Si-O species results in a new peak at shorter Si-O distances.

SUMMARY AND CONCLUSION

Reactive molecular dynamic (RMD) simulations are carried out to investigate the effect of temperature and electric field (EF) on the nucleation and binding (growth) of silica nanoparticles (NPs) in the flame synthesis process by defining two A and B systems with different compositions. For the system A, starting with TMOS, SiO_2, O_2 and Ar species, it was noticed that TMOS decomposition becomes faster by increasing temperature and conversion of TMOS to small Si_mO_n species is most favored at 1500 K. The formation of silica initial seeds (as the first step of the nucleation of SiO_2 NPs) in the flame synthesis process is successfully simulated by this RMD simulation. Close inspection of all processes in the simulation, especially by following the conversion reactions of TMOS to Si_mO_n, shows that the first step which opens the route towards the reaction products is the production of the $SiO_3C_3H_9$ species, in which they lose their carbon and hydrogen atoms to produce the primary Si_mO_n seeds in the later stages of the reaction.

By increasing the flame temperature in the absence of external EF, the collision and attachment of particles are increased and thus larger NPs with broader size distribution are produced. Results of the simulations on the system B at 2100 K temperature show that weak external EFs (around 1 V/Å) prevent silica NPs from binding to each other, while moderate EFs (4-6 V/Å) not only prevent attachment of silica NPs, but facilitate decomposition of the smaller NPs. In strong EFs (7 & 8 V/Å), silica NPs are not stable and are completely decomposed to small atomic clusters, molecules, and atoms. At 2100 K temperature, application of weak EFs, makes the size distribution of the silica NPs narrower. At very high temperature 3300 K, thermal decomposition and attachment of NPs are the two competing driving forces which interplay results in a wider size distribution of the NPs. As a general conclusion, in the flame synthesis of SiO_2 nanoparticles, smaller NPs with narrower size distribution

can be achieved by applying external EF with certain strength depending on the temperature of the flame medium. Structure of the silica NPs is investigated by calculating and analyzing different Si-Si, Si-O and O-O atomic pairs radial distribution functions (RDF). These RDFs indicate that the silica NPs formed in these reactive simulations have amorphous phase.

As presented in this report, our study has been successful in providing an initial picture of this complex reactive system. A complete picture can only be achieved in multi-scale multi-stage kinetics, dynamics, diffusive and convective simulations which is not easily applicable at this time with our limited expertise and hardware facilities.

SUPPORTING INFORMATION

Time variations of the number of C-O and C-H bonds in the system A (Fig. S1) and calculated RDFs at different temperatures and electric field strengths (Fig. S2), and the number of Si-H, O-H and Si-O bonds in the system B at the final step of the simulations (Figs. S3 and S4) and the snapshots of the system B configuration at the end of the simulations in different EF strengths (Fig. S5) are presented in Supporting Information. Furthermore, some animations of the A and B systems at T = 2100 K and EF = 2 V/Å conditions are also attached to the Supporting Information file.

ACKNOWLEDGEMENTS

We thank Dr. van Duin for generously providing us with the ReaxFF software, and useful explanation and introduction of some features of the ReaxFF force field and the software options. We also thank Dr. Axel Kohlmeyer for his guidance on solving problems with installation and settings of the LAMMPS software. Financial supports from the Iranian Nanotechnology Initiative Council, and the Research and Technology Office of the University of Isfahan are acknowledged.

REFERENCES

[1] Lindsay, S. M., Introduction to Nanoscience. Oxford, 2010, pp. 1-10.

[2] Cao, G., Nanostructures & Nanomaterials. Imperial College Press, 2004, pp. 8-13.

[3] Rezapour, M.; Mirzaei, A.; Zohdi-Fasaei, H., Optimizing the preparation conditions of silica supported Fe-Co-Ce ternary catalyst for the fixed-bed Fischer-Tropsch synthesis: Taguchi experimental design approach. *Phys. Chem. Res.* **2018**, *6*, 387-397, DOI: 10.22036/pcr.2018.118835.1467.

[4] Hashemzehi, H.; Mirzaei, A.; Atashi, H.; Rezaeian, F., Preparation of iron-cobalt-cerium heterogeneous nano-catalysts to produce light hydrocarbons from synthesis gas. *Phys. Chem. Res.* **2018**, *6*, 785-794, DOI: 10.22036/pcr.2018.127286.1479.

[5] Ashassi-Sorkhabi, H.; Rezaei-moghadam, B.; Bagheri, R.; Abdoli, L.; Asghari, E., Synthesis of Au nanoparticles by thermal, sonochemical and electrochemical methods: optimization and characterization. *Phys. Chem. Res.* **2015**, *3*, 24-34, DOI: 10.22036/pcr.2015.7311.

[6] Azizi Toupkanloo, H.; Fathollahi, M., Molecular dynamics simulation of Al/NiO thermite reaction using reactive force field (ReaxFF). *Phys. Chem. Res.* **2017**, *5*, 221-237, DOI: 10.22036/pcr.2017.40619.

[7] Sabzyan, H.; Taghavi, F., Theoretical study of magnetic susceptibility and optical activity of small molecules containing one chiral center. *Phys. Chem. Res.* **2014**, *2*, 41-52, DOI: 10.22036/pcr.2014.3859.

[8] Gun'ko, V. M.; Zarko, V. I.; Voronin, E. F.; Turov, V. V.; Mironyuk, I. F.; Gerashchenko, E. V.; Goncharuk, E. V.; Pakhlov, E. M.; Guzenko, N. V., Impact of some organics on structural and adsorptive characteristics of fumed silica in different media. *J. Am. Chem. Soc.* **2002**, *18*, 581-596, DOI: 10.1021/la0103867.

[9] Li, C.; Hu, Y.; Yuan, W., Nanomaterials synthesized by gas combustion flames: morphology and structure. *Institute Process Eng.* **2010**, *8*, 556-562, 10.1016/j.partic.2010.08.009.

[10] Yue, R.; Meng D.; NI, Y.; Liu, G.; Yang, J.; Liu, H.; Wu, X.; Chen, Y., One-step flame synthesis of hydrophobic silica nanoparticles. *Powder Technol.* **2013**, *235*, 909-913, DOI: 10.1016/j.powtec.2012.10.021.

[11] Kammler, H. K.; Mädler, L.; Pratsinis, S. E., Flame

synthesis of nanoparticles. *Chem Eng Technol.* **2001**, *24*, 583-606, DOI: 10.1002/1521-4125(200106).

[12] Acosta, S.; Quintanilla, L.; Alonso, M.; Aparicio, C.; Rodríguez-Cabello, J. C., Recombinant AMP/ polypeptide self-assembled monolayers with synergistic antimicrobial properties for bacterial strains of medical relevance. *Am. Chem. Soc.* **2019**, *5*, 4708-4716, DOI: 10.1021/acsbiomaterials.9b00247.

[13] Vistoli, L.; Wang, W.; Sander, A.; Zhu, Q.; Casals, B.; Cichelero, R., Giant topological Hall effect in correlated oxide thin films. *Nature Phys.* **2019**, *15*, 67-72, DOI: 10.1038/s41567-018-0307-5.

[14] Torres-Cavanillas, R.; Sanchis-Gual, R.; Dugay, J.; Coronado-Puchau, M.; Giménez-Marqués, M., Design of bistable gold@spin-crossover core-shell nanoparticles showing large electrical responses for the spin switching. *Adv. Mat.* **2019**, *31*, 19-39, DOI: 10.1002/adma.201900039.

[15] Harrison, J. A.; Schall, J. D.; Maskey, S.; Mikulski, P. T.; Knippenberg, M. T.; Morrow, B. H., Review of force fields and intermolecular potentials used in atomistic computational materials research. *Appl. Phys. Rev.* **2018**, *5*, 31104-31129, DOI: 10.1063/ 1.5020808.

[16] Senftle, T. P.; Hong, S.; Islam, M. M.; Verstraelen, T.; Grama, A.; van Duin, A. C. T., The ReaxFF reactive force-field: development, applications and future directions. *NPJ Comput. Mater.* **2016**, *2*, 15011-15025, DOI: 10.1038/npjcompumats.2015.11.

[17] Jensen, B. D.; Wise, K. E.; Odegard, G. M., Simulation of the elastic and ultimate tensile properties of diamond, graphene, carbon nanotubes, and amorphous carbon using a revised ReaxFF parametrization, *J. Phys. Chem. A* **2015**, *119*, 9710-9721, DOI: 10.1021/acs.jpca.5b05889.

[18] Neyts, E. C.; Shibuta, Y.; Van Duin, A. C.; Bogaerts, A., Catalyzed growth of carbon nanotube with definable chirality by hybrid molecular dynamics-force biased Monte Carlo simulations, *ACS Nano,* **2010**, *4*, 6665-6672, DOI: 10.1021/nn102095y.

[19] Shekar, S.; Sander, M.; Riehl, R. C.; Smith, A. J.; Braumann, A.; Kraft, M., Modelling the flame synthesis of silica nanoparticles from tetraethoxysilane. *Chem. Eng. Sci.* **2012**, *70*, 54-66, DOI: 10.1016/j.ces.2011.06.010.

[20] Grosschmidt D.; Bockhorn H.; Goodson M.; Kraft M., Two approaches to the simulation of silica particle synthesis. *Proc. Combust. Inst.* **2002**, *29*, 1039-1046, DOI: 10.1016/S1540-7489(02)80131-6.

[21] Floess, J. K., Murad, S., Molecular simulations of the competitive adsorption of siloxanes and water on amorphous silica surfaces as a function of temperature. *Chem. Phys. Lett.* **2011**, *516*, 216-219, DOI: 10.1016/j.cplett.2011.09.085.

[22] Flikkema, E.; Jelfs, K. E.; Bromley, S. T., Structure and energetics of hydroxylated silica clusters. $(SiO_2)M(H_2O)N$, M = 8, 16 and N = 1-4: A global optimization study. *Chem. Phys. Lett.* **2012**, *554*, 117-122, DOI: 10.1016/j.cplett.2012.10.016.

[23] Kirk, S. R.; Yin, D.; Persson, M.; Carlen, J.; Jenkins, S., Molecular dynamics simulations of the aggregation of nanocolloidal amorphous silica monomers and dimers. *Procedia Eng.* **2011**, *18*, 188-193, DOI: 10.1016/j.proeng.2011.11.030.

[24] Smith, J. S.; Borodin, O.; Smith, G. D.; Kober, E. M., A molecular dynamics simulation and quantum chemistry study of poly(dimethylsiloxane)-silica nanoparticle interactions. *J. Polym. Sci., Part B: Polym. Phys.* **2007**, *45*, 1599-1615, DOI: 10.1002/ polb.21119.

[25] van Duin, A. C. T.; Alejandro, S.; Shannon, S.; Zhang, Q.; Xu, X.; Goddard, W. A., ReaxFFSiO reactive force field for silicon and silicon oxide systems. *J. Phys. Chem. A* **2003**, *107*, 3803-3811, DOI: 10.1021/jp0276303.

[26] Fogarty, J. C.; Aktulga, H. M.; van Duin, A. C. T.; Grama, A. Y.; Pandit, S. A., A reactive molecular dynamics simulation of the silica-water interface. *J. Chem. Phys.* **2010**, *132*, 174704-174714, DOI: 10.1063/1.3407433.

[27] Pamungkas, M. A.; Joe, M.; Kim, B.; Lee, K., Reactive molecular dynamics simulation of early stage of dry oxidation of Si (100) surface. *J. Appl. Phys.* **2011**, *110*, 53513-53520, DOI: 10.1063/ 1.3632968.

[28] Kim, B. H.; Jung, H.; Chung, Y.; Shin, M.; Lee, K., Multi-scale simulation of interfacial roughness effects in silicon nanowires. *SISPAD Conference Series*

2012, *2*, 5-7, DOI: 10203/173358.

[29] Nayir, N.; van Duin, A. C.; Erkoc, S., Development of the ReaxFF Reactive Force Field for Inherent Point Defects in the Si/Silica System. *J. Phys. Chem. A* **2019**, 123, 4303-4313, DOI: 10.1021/acs.jpca.9b01481.

[30] Chenoweth, K.; van Duin, A. C. T.; Cheung, S.; Goddard III, W. A.; Kober, E. M., Simulations on the thermal decomposition of a poly(dimethylsiloxane) polymer using the ReaxFF reactive force field. *J. Am. Chem. Soc.* **2005**, *127*, 7192-7202, DOI: 10.1021/ja050980t.

[31] Rahnamoun, A.; van Duin, A. C. T., Study of ice cluster impacts on amorphous silica using the ReaxFF reactive force field. *J. Appl. Phys.* **2016**, *119*, 95901-95910, DOI: 10.1063/1.4942997.

[32] Rimsza, J. M.; Yeon, J.; van Duin, A. C. T.; Du, J., Water interactions with nanoporous silica: comparison of ReaxFF and *ab Initio* based molecular dynamics simulations. *J. Phys. Chem. C* **2016**, *120*, 24803-24816, DOI: 10.1021/acs.jpcc.6b07939.

[33] Rimsza, J. M.; Du, J., Interfacial structure and evolution of the water-silica gel system by reactive force-field-based molecular dynamics simulations. *J. Phys. Chem. C* **2017**, *121*, 11534−11543, DOI: 10.1021/acs.jpcc.7b02734.

[34] Yeon, J., van Duin, A. C. T., ReaxFF molecular dynamics simulations of hydroxylation kinetics for amorphous and nano-silica structure, and its relations with atomic strain energy. *J. Phys. Chem. C* **2016**, *120*, 305-317, DOI: 10.1021/acs.jpcc.5b09784.

[35] Kammler, H. K.; Jossen, R.; Morrison, P. W.; Pratsinis, S. E.; Beaucage, G., The effect of external electric fields during flame synthesis of titania. *Powder Technol.* **2003**, *135*, 310-320, DOI: 10.1016/j.powtec.2003.08.023.

[36] Vemury, S.; Pratsinis, S. E., Corona-assisted flame synthesis of ultrafine titania particles. *Appl. Phys. Lett.* **1995**, *66*, 3275-3277, DOI: 10.1063/1.113402.

[37] Morrison, P. W.; Raghavan, R.; Timpone, A. J., In situ Fourier transforms infrared characterization of the effect of electrical fields on the flame synthesis of TiO_2 particles. *Chem. Mater.* **1997**, *9*, 2702-2708, DOI: 10.1021/cm960508u.

[38] Merchan-Merchan, W.; Saveliev, A. V.; Kennedy, L. A., High-rate flame synthesis of vertically aligned carbon nanotubes using electric field control. *Carbon* **2004**, *42*, 599-608, DOI: 10.1016/j.carbon.2003.12.086.

[39] Dai, H., Carbon nanotubes: synthesis, integration, and properties. *Acc. Chem. Res.* **2002**, *35*, 1035-1044, DOI: 10.1021/ar0101640.

[40] Kammler, H. K.; Pratsinis, S. E., Electrically-assisted flame aerosol synthesis of fumed silica at high production rates. *Chem. Eng. Process.* **2000**, *39*, 219-227, DOI: 10.1016/S0255-2701(99)00082-3.

[41] Spicer, P. T.; Artelt, C.; Sanders, S.; Pratsinis, S. E., Flame synthesis of composite carbon black-fumed silica nanostructured particles. *J. Aerosol Sci.* **1998**, *29*, 647-659, DOI: 10.1016/S0021-8502(97)10023-4.

[42] Hyeon-Lee, J.; Beaucage, G.; Pratsinis, S. E.; Vemury, S., Fractal analysis of flame-synthesized nanostructured silica and titania powders using small-angle x-ray scattering. *J. Am. Chem. Soc.* **1998**, *14*, 5751-5756, DOI: 10.1021/la980308s.

[43] Neyts, E. C.; van Duin A. C. T.; Bogaerts, A., Insights in the plasma-assisted growth of carbon nanotubes through atomic scale simulations: effect of electric field. *J. Am. Chem. Soc.* **2011**, *134*, 1256-1260, DOI: 10.1021/ja2096317.

[44] Wood, M. A.; van Duin, A. C. T.; Strachan, A., Coupled thermal and electromagnetic induced decomposition in the molecular explosive αHMX; a reactive molecular dynamics study. *J. Phys. Chem. A* **2013**, *118*, 885-895, DOI: 10.1021/jp406248m.

[45] Vemury, S.; Pratsinis, S. E., Charging and coagulation during flame synthesis of silica. *J. Aerosol Sci.* **1996**, *27*, 951-966, DOI: 10.1016/0021-8502(96)00040-7.

[46] Vemury, S.; Pratsinis, S. E.; Kibbey, L., Electrically controlled flame synthesis of nanophase TiO_2, SiO_2, and SnO_2 powders. *J. Mater. Res.* **1997**, *12*, 1031-1042, DOI: 10.1557/JMR.1997.0144.

[47] Fan, Y.; Li, X.; Jang, S. H.; Lee, D. H.; Li, Q.; Cho, U. R., Reinforcement of solution styrene-butadiene rubber by incorporating hybrids of rice bran carbon and surface modified fumed silica. *J. Vinyl. Addit. Technol.* **2018**, *24*, 1-7, DOI: 10.1002/vnl.21635.

[48] Rwei, S. P.; Shiu, J. W.; Sasikumar, R.; Hsueh, H. C.,

Characterization and preparation of carbonyl iron-based high magnetic fluids stabilized by the addition of fumed silica. *J. Solid State Chem.* **2019**, *274*, 308-314, DOI: 10.1016/j.jssc.2019.03.039.

[49] Santos, J.; Calero, N.; Trujillo-Cayado, L. A.; Muñoz, J., Development and characterisation of a continuous phase based on a fumed silica and a green surfactant with emulsion applications. *Colloids Surf. A* **2018**, *555*, 351-357, DOI: 10.1016/j.colsurfa.2018.07.017.

[50] Larsson, H. L.; van Duin, A. C. T.; Hartke, B., Global optimization of parameters in the reactive force field ReaxFF for SiOH. *J. Comp. Chem.* **2013**, *34*, 2178-2189, DOI: 10.1002/jcc.23382.

[51] Visit the official website of LAMMPS at https://lammps.sandia.gov/

[52] Mahajan, S. M.; Subbarayan, G.; Sammakia, B. G., Estimating thermal conductivity of amorphous silica nanoparticles and nanowires using molecular dynamics simulations. *Phys. Rev. E* **2007**, *76*, 56701-56714, DOI: 10.1103/PhysRevE.76.056701.

[53] McQuarrie, D. A., Statistical Mechanics. Harper & Row: 1976, p. 255-279.